A Light and Scanning Electron Microscopy Study of Human Direct Laser Metal Forming Dental Implants

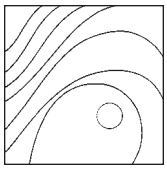

Carlo Mangano, MD, DDS[1]/Adriano Piattelli, MD, DDS[2]/ Antonio Scarano, MD, DDS, MS[3]/Mario Raspanti, MS[4]/ Jamil A. Shibli, DDS, PhD[5]/Francesco G. Mangano, DDS[6]/ Vittoria Perrotti, DDS, PhD[7]/Giovanna Iezzi, DDS, PhD[8]

Direct laser metal forming (DLMF) is a procedure in which a high-power laser beam is directed on a metal powder bed and programmed to fuse particles according to a computer-aided design file, thus generating a thin metal layer. With DLMF, it is now possible to fabricate dental implants with a superficial porous surface. The aim of the present study was to evaluate the peri-implant soft tissues around human-retrieved DLMF dental implants. Collagen fibers, in the form of bundles, were oriented perpendicularly to a distance of 100 µm from the surface, where they became parallel, running in several directions. In some portions, only a few collagen fiber bundles appeared to be oriented perpendicularly or obliquely to the plane of the section. Collagen fibers appeared to form a dense chaotic three-dimensional network running in different, more or less parallel directions to the surface. Under scanning electron microscopy, an intimate contact of the fibrous matrix with the implant surface was evident, and some collagen bundles could be seen to bind directly to the metal surface. By changing the surface microtexture, it was possible to change the response of the peri-implant soft tissues. (Int J Periodontics Restorative Dent 2014;34:e9–e17. doi: 10.116047/prd.1213)

[1]Researcher, Department of Surgical and Morphological Sciences, Dental School, University of Varese, Como, Italy.
[2]Professor, Department of Medical, Oral and Biotechnological Sciences, Dental School, University of Chieti-Pescara, Italy.
[3]Associate Professor, Department of Medical, Oral and Biotechnological Sciences, Dental School, University of Chieti-Pescara, Italy.
[4]Professor, Department of Human Anatomy, Medical School, University of Varese, Como, Italy.
[5]Head, Oral Implantology Clinic; Associate Professor, Department of Periodontology, Dental Research Division, Guarulhos University (UnG), Guarulhos, Sao Paulo, Brazil.
[6]Private Practice, Gravedona, Como, Italy.
[7]Research Fellow, Department of Medical, Oral and Biotechnological Sciences, Dental School, University of Chieti-Pescara, Italy.
[8]Researcher, Department of Medical, Oral and Biotechnological Sciences, Dental School, University of Chieti-Pescara, Italy.

Correspondence to: Prof Carlo Mangano, Piazza Trento 4, 22015 Gravedona (Como), Italy; email: camangan@gmail.com.

The soft tissues around dental implants play a relevant role in the defense of the bone from oral bacteria.[1] The establishment of a firm functional soft tissue barrier is considered to be important to protect the implant interface from the invasion of bacteria from the oral cavity.[1,2] Moreover, the peri-implant soft tissue resistance to mechanical forces during mastication may influence the long-term esthetic appearance.[1] Biologic width (BW) is the distance from the mucosal margin to the alveolar bone.[1] This BW around teeth shows a constant vertical dimension[3] and is constituted by the sulcular epithelium (SE), the junctional epithelium (JE), and the connective tissue (CT). The supracrestal peri-implant soft tissues around implants appear to be similar to the tissues around the teeth and also form a BW composed of epithelium and CT.[4,5] The only difference is the lack of attachment of CT fibers to the implant surface.[6] Due to this fact, most fibers in CT run in a direction more or less parallel to the implant surface.[7] The presence of a direct fiber attachment to dental implants has been debated in the literature.[7] The

absence of a real CT attachment to the implant surface has been postulated.[1] A perpendicular orientation to the implant surface may result in better anchorage to the metal.[7] The attachment of functionally oriented CT would impede the apical migration of the JE and preserve the crestal bone level.[6,7] Changes in the surface microscopic texture can be used to change the response of the peri-implant bone and soft tissue.[6] The presence of microgrooves or other three-dimensional (3D) surface geometries could help establish direct fibrocollagenous attachment, limiting the apical migration of the epithelium.[8] Fibers directed perpendicularly to the implant surface have been described in microtextured surfaces,[7] and only in the oxidized surface have collagenous fibers become functionally oriented and appeared to extend more or less perpendicularly into the implant surface.[7] The mechanical interlocking of the collagen fibers into the pores of the oxidized implants may help with fiber anchorage.[7]

Direct laser metal forming (DLMF) is a metal-forming procedure in which a high-power laser beam is directed onto a metal powder bed and programmed to fuse particles according to a computer-assisted design (CAD) file, thus generating a thin metal layer.[9–13] The apposition of subsequent layers gives shape to a desired 3D form with minimal postprocessing requirements. With DLMF, it is now possible to fabricate dental implants with different shapes and surface microcharacteristics directly from the CAD models.[9–13] With this technique, it is possible to obtain functionally graded titanium implants with a porosity gradient perpendicular to the implant's long axis. Furthermore, in DLMF, a superficial porous surface structure is obtained.[9–13]

The aim of the present light and scanning electron microscopy (SEM) study was an evaluation of the peri-implant soft tissues around human-retrieved DLMF one-piece implants.

Method and materials

Selection of subjects

Twelve totally edentulous subjects (8 women, 4 men), with a mean age of 56.45 ± 2.01 years, referred to the Oral Implantology Clinic, Guarulhos University (UnG), Brazil, for oral rehabilitation with dental implants were included in this study. Exclusion criteria included subjects who were pregnant, nursing, or smokers and those with any systemic condition that could affect bone healing. The Ethics Committee for Human Clinical Trials at Guarulhos University approved the study protocol (CEP-UnG no. 201).

Preparation of the DLMF implants

Implants were manufactured with the DLMF technique (TixOs Nano Ovd, Leader-Novaxa). The DLMF implants were made of master alloy powder (Ti-6Al-4V), with a particle size of 25 to 45 µm as the basic material. Processing was carried out in an argon atmosphere using a powerful Yb (ytterbium) fiber laser system (Eos Laser Systems) with the capacity to build a volume up to 250 × 250 × 215 mm using a wavelength of 1,054 nm with a continuous power of 200 W, at a scanning rate of 7 m/s. The size of the laser spot was 0.1 mm. To remove residual particles from the manufacturing process, the sample was sonicated for 5 minutes in distilled water at 25°C, immersed in sodium hydroxide (20 g/L) and hydrogen peroxide (20 g/L) at 80°C for 30 minutes, and then further sonicated for 5 minutes in distilled water. Acid etching was carried out by immersion of the samples in a mixture of 50% oxalic acid and 50% maleic acid at 80°C for 45 minutes, followed by washing for 5 minutes in distilled water in a sonic bath. The surface topography of the DLMF implants had no clear orientation. The direct laser preparation provided an implant surface with a very high roughness. The peak-to-valley difference (Sz), measured as the mean height of the five highest points minus the mean height of the five lowest points, was 358.3 ± 101.9 µm. The mean of the absolute values of all profile points (Sa) was 66.8 ± 6.6 µm, while the root mean square (RMS) of the value of all points (Sq) was 77.6 ± 11.1 µm. One-piece screw-shaped implant (2.5 mm in diameter and 6 mm in length) surfaces were prepared using direct laser metal sintering. To evaluate the behavior of the peri-implant soft tissue,

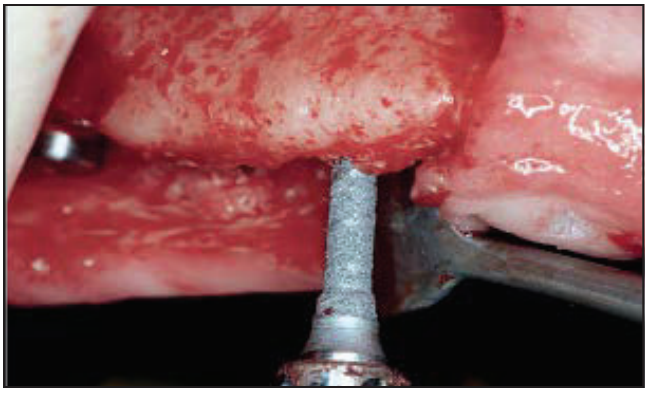

Fig 1 *Tixos implant during insertion.*

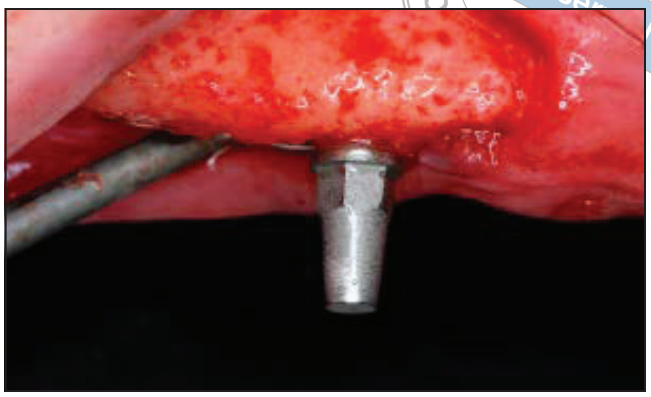

Fig 2 *The implant was placed with the neck at the level of the crestal bone.*

the neck of the implants presented two different surface topographies: DLMF topography (test group) and acid-etched surface topography only (control group). Finally, the implants were sterilized using gamma radiation.

Microimplant surgery

Twenty-four microimplants were used in this study. Each subject received two microimplants (one test and one control in a split-mouth design), which were inserted in the posterior region of the maxilla, always distal to the last conventionally placed implant.

The microimplants were placed under aseptic conditions as previously described (Fig 1).[12] After crestal incision, mucoperiosteal flaps were raised and conventional implants were placed in the totally edentulous maxilla in accordance with the surgical/prosthetic plan prepared for each patient (Fig 2). Next, the micro-implant was randomly placed in the molar region, ie, posterior to the most distal conventional implant. The microimplant recipient site was prepared with a 1.8-mm-diameter twist drill in soft bone. All drilling and microimplant placement procedures were completed under profuse irrigation with sterile saline. If the microimplant showed low primary stability, a backup surgical site was prepared. The flaps were sutured to allow the emergence of the one-piece implant through the mucosa. Clindamicin was administered three times a day (1,200 mg/day) for 1 week to avoid postsurgical infection. The sutures were removed after 10 days. To enable subjects to control postoperative dental biofilm, 0.12% chlorhexidine rinses were prescribed, twice a day, for 14 days.

Specimen retrieval

After a healing period of 8 weeks, during stage-two surgery of the conventionally placed implants, the microimplants and the surrounding tissues were retrieved with a 4.0-mm-wide trephine bur, and the specimens were fixed by immediate immersion in neutral formalin at 4%. Part of the specimens was washed with sodium-cacodylate buffer (pH 7.4), dehydrated in ascending ethanol and hexamethyldisilazane, sputter-coated with pure gold in an Emitech K550 apparatus, and mounted on appropriate stubs with a carbon-based conductive adhesive. All specimens were observed under an FEI XL-30 FEG scanning electron microscope (SEM) operated at 7 to 15 kV. Pictures were acquired in digital format as 1,424 × 968-pixel grayscale TIFF images. Other specimens were processed to obtain thin ground sections.

Table 1 Soft tissue measurements

Tissue	Mean ± SD (mm)
Sulcular epithelium	1.1 ± 0.9
Junctional epithelium	1.2 ± 0.3
Connective tissue	1.5 ± 0.5

Processing of specimens

The implants and surrounding tissues were immediately stored in 10% buffered formalin and processed to obtain thin ground sections (Precise 1 Automated System, Assing).[14] The specimens were dehydrated in an ascending series of alcohol rinses and embedded in a glycolmethacrylate resin (Technovit 7,200 VLC, Kulzer). After polymerization, the specimens were sectioned longitudinally along the major axis of the implants with a high-precision diamond disk at approximately 150 µm and ground to approximately 30 µm. Three slides were obtained. The slides were stained with basic fuchsin and toluidine blue. A double staining with von Kossa and acid fuchsin was done to evaluate the degree of bone mineralization. One slide, after polishing, was immersed in silver nitrate ($AgNO_3$) for 30 minutes, and exposed to sunlight. The slides were then washed under tap water, dried, immersed in basic fuchsin for 5 minutes, and washed and mounted. The slides were observed under a Leitz Laborlux microscope. Some slides were carbon-coated and also observed using SEM in backscattered electron detection (BSE).

Results

All implants appeared to have osseointegrated from a clinical point of view, and mobility was absent.

Light microscopy

The SE was composed of 4 to 5 layers of parakeratinized epithelial cells and had a length of 1.2 to 1.3 mm. The JE was composed of 4 to 5 layers of epithelial cells and had a length of 1.0 to 1.5 mm (Fig 3). The CT attachment had a width of between 1.0 to 2.1 mm (Table 1). Under polarized light it was possible to note the parallel arrangement of the collagen fibers near the abutment surface (Fig 4). Collagen fibers, in the form of bundles, were oriented perpendicularly up to a distance of 100 µm from the surface where they became parallel, running in several directions. In some portions, collagen fiber bundles appeared to be oriented perpendicularly or obliquely to the plane of the section (Figs 5 and 6). Collagen fibers appeared to form a dense chaotic 3D network running in different, more or less parallel directions to the surface (Fig 6). Monocytes and macrophages were present in only a few areas. However, no acute or chronic inflammatory cell infiltrate was present. Elongated fibroblasts were observed in some portions of the specimens. No epithelial downgrowth was present in any of the specimens. In the portion near the surface of the abutment, only a few blood vessels were found in the CT.

SEM

The integrated specimen appeared as a cylinder of bone, fibrous tissues, and vascular structures enclosing the metal implant. Since the SEM could only visualize surfaces and could not reach the interior of the specimen, a part of the implant was freed of the host tissues to obtain unobstructed access to the implant-matrix interface. The surface of the implant was characterized by a disordered succession of irregular, rounded protrusions, narrow crevices, and intercommunicating pores. The mechanical bond of the host tissues with the implant was tight enough for the tissues to remain in place when the overlaying tissue was torn away during specimen preparation. All surface features appeared covered in a dense connective matrix crisscrossing around the protrusions of the implant and randomly interweaving inside its voids and crevices. The rounded, pebble-like protrusions of the implant were easily recognizable in SEM imaging, but they were even more highlighted by the BSE imaging mode, where the metal appeared much brighter than the

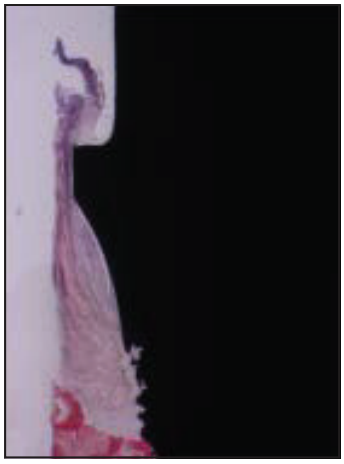

Fig 3 (left) *The SE was composed of parakeratinized epithelial cells and had a length of about 1.2 to 1.3 mm. The JE had a length of about 1.0 to 1.5 mm. CT attachment was 1.2 mm (toluidine blue–basic fuchsin; original magnification ×50).*

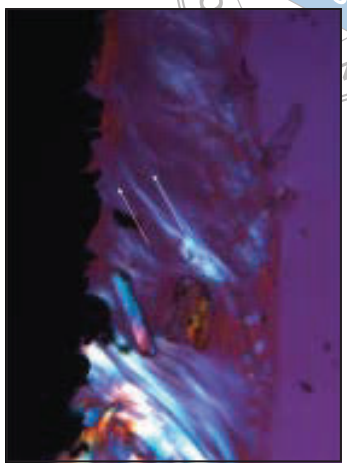

Fig 4 (right) *Under polarized light, it was possible to see that the collagen fibers had a parallel arrangement* (arrows) *near the abutment surface (toluidine blue–basic fuchsin; original magnification ×50).*

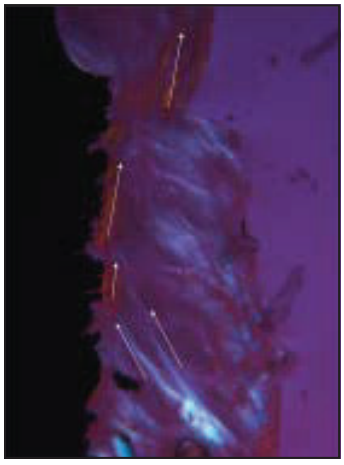

Fig 5 (left) *Under polarized light, it was possible to see that the collagen fibers, in the form of bundles, were oriented perpendicularly to the abutment surface, up to a distance of 100 µm from the surface, where they became parallel running* (arrow) *in several directions (toluidine blue–basic fuchsin; original magnification ×50).*

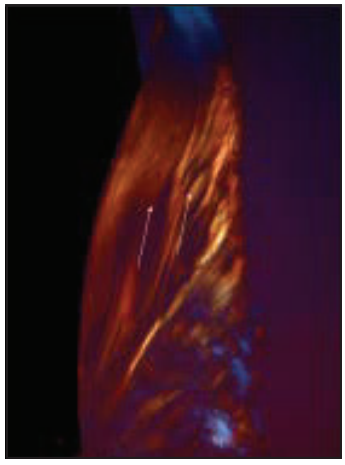

Fig 6 (right) *Higher magnification of yellow area of previous image. Collagen fibers appeared to form a dense chaotic 3D network running in different but more or less parallel directions to the surface (original magnification ×100).*

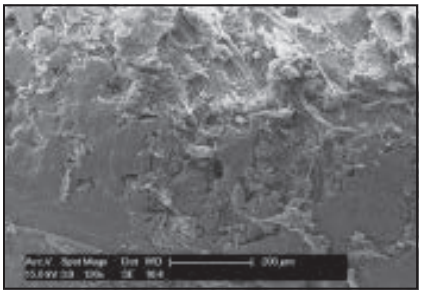

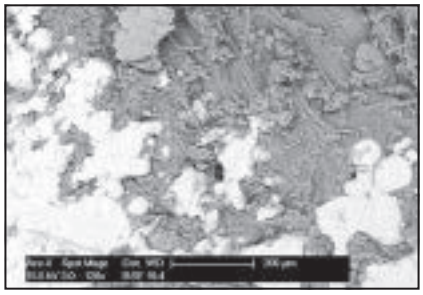

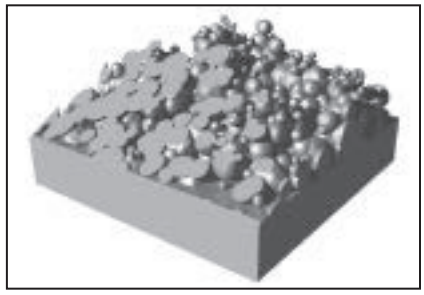

Fig 7 (a) *Low-magnification SEM micrograph showing the soft fibrous tissue interweaving with the surface protrusions of the implant surface, which were partly cut off during the implant extraction.* (b) *The same field of view now seen in BSE. This technique highlights the metal (bright) and allows for an easier discrimination from the surrounding soft tissue.* (c) *A schematic computer model of the native Tixos implant surface, cut obliquely to show the aspect of a grazing section corresponding to the preceding images.*

organic matrix (Fig 7). Close to the implant surface, the collagen bundles did not show a preferential orientation (Figs 8 and 9) but always remained closely connected to the metal surface. At a higher magnification, the intimate contact of the fibrous matrix with the implant surface became evident, and some collagen bundles were directly bound to the metal surface (Fig 10). An exception was represented by

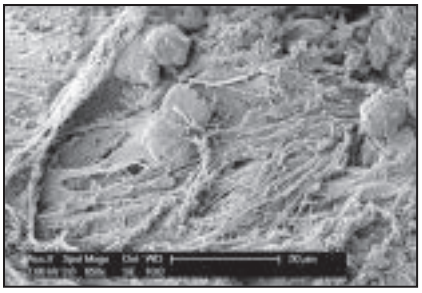

Fig 8 *Higher-magnification SEM micrograph of the host/implant interface. The spheroidal particles residuating from the sintering process emerge from a dense network of collagen fibers.*

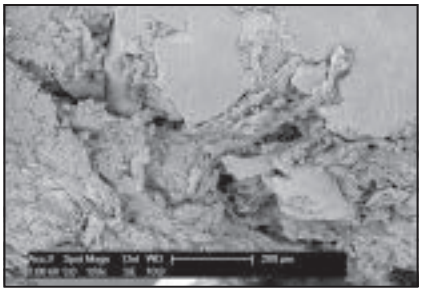

Fig 9 *Where the surface features of the implant were cut during the implant recovery, it is possible to follow the growth and the adhesion of the collagen strands into the narrowest crevices.*

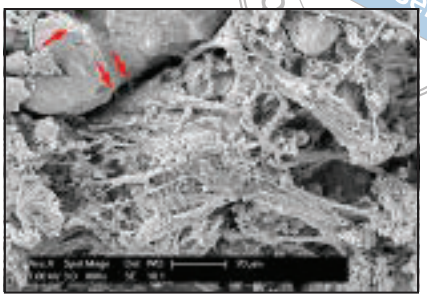

Fig 10 *A detail of the interface. At this magnification, the metal surface begins to reveal its microcrystalline nature. The implant portions emerging from the extracellular matrix are immediately evident. A few collagen strands can be seen to bind directly onto the implant* (arrows).

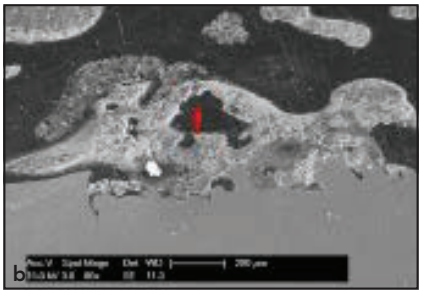

Fig 11 (a) *A ground section observed in light microscopy in polarized light. The dense CT of bone is brightly refringent and even displays the dark cross distinctive of a mature osteon* (arrow). (b and c) *The SEM observation of the same field of view reveals a little more detail, as a Howship resorption lacuna* (arrow). *The soft tissues are scarcely visible in both cases.*

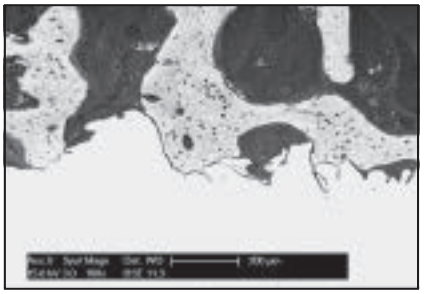

Fig 12 *A ground section treated with uranyl acetate and observed in BSE. In decreasing order of brightness, the implant, bone, and soft tissues can be found.*

the smooth, machined neck of the implant, where the adhesion was lower and the connective matrix was entirely detached by the specimen preparation procedure. SEM observation of ground sections initially prepared for light microscopy was able to yield pictures of the implant and surrounding bone superimposable with this latter technique (Fig 11). The imaging of soft tissues required, however, a specific treatment with heavy metal salts. This approach revealed the uncalcified extracellular matrix, soft tissues, and vascular structures with greater intelligibility (Fig 12). In particular, the connective fiber bundles appeared as bright, soft, smoky traces waving among the surface protrusions and sometimes directly binding to the metal surface (Fig 13). On the implant neck, this approach was less traumatic and maintained intact the gingival seal, as can be seen both under light microscopy and SEM (Fig 14).

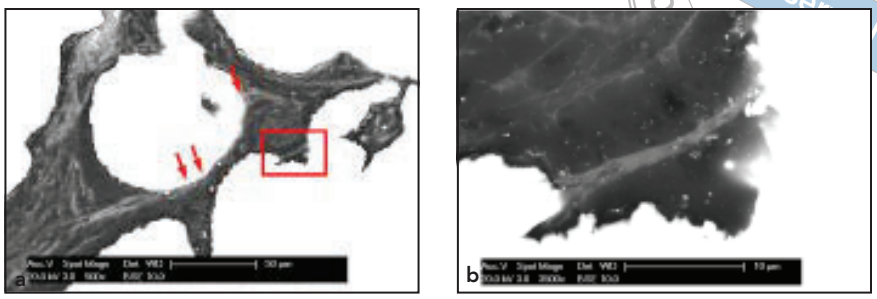

Fig 13 (a) *At higher magnification, the strands of soft tissue are more appreciable and appear as soft undulating streaks. Again, in some cases they can be seen to connect directly to the specimen surface* (arrows). (b) *The framed area is depicted at higher magnification.*

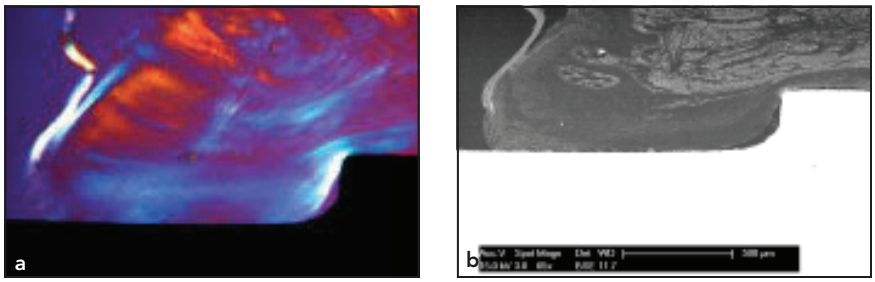

Fig 14 *The smooth machined part of the implant has a simpler surface and a weaker adhesion with the surrounding matrix. These micrographs (left, polarized light microscopy; right, SEM) show the regular structure of the gingival seal around the emerging portion of the implant.*

Discussion

The soft tissue barrier around implants provides an essential biologic and physiologic barrier to protect bone anchorage. Recently, many studies have focused on the morphologic features of the epithelium and CT around implants. Most of the histologic studies found in the literature on peri-implant soft tissues involved animals.[15] The results of animal studies do not always correspond to the biologic behavior of soft tissues in the humans.[1] Few studies have investigated human peri-implant soft tissues.[5,16] Human histologic data are valuable to validate and confirm the data from animal models.[5] A rough surface may have a conductive effect on CT adhesion during healing, inhibiting epithelial downgrowth.[1] The preservation of stable relationships between overlying soft tissues and the underlying supporting crestal bone is critical for optimal form and function.[8] Gargiulo et al[17] found that BW was a physiologically formed and stable dimension around teeth. BW around implants is needed to ensure adequate JE and CT to obtain an optimal seal,[18] and its dimension has been reported to be dependent on the presence/absence of the implant-abutment junction microgap and on the location of this microgap relative to the alveolar crest.[15–20] In an autopsy case report, the length of the JE was found to be 3.00 mm,[16] while Glauser et al[1], in a study on retrieved microimplants, found different lengths depending on the surface structure of the abutment: 1.8 mm in oxidized abutments, 1.9 mm in acid-etched abutments, and 3.4 mm in machined abutments. Also, the loading conditions of the implants probably influence the length of the JE: Cochran et al[21] reported 1.16 mm for unloaded implants, 1.44 mm for implants loaded for a 3-month period, and

1.86 mm for implants loaded for 12 months. Additionaly, the surface characteristics of the abutment appear to have a role in CT organization, and Glauser et al[1] reported, in a human study on retrieved microimplants after an unloaded transmucosal healing of 8 weeks, 2.1 mm for an oxidized surface, 2.6 mm for an acid-etched surface, and 3.4 mm for a machined surface. These results confirm those reported by Siar et al[4] and by Quaranta et al[22] in experimental studies in monkeys. The supracrestal CT was, in animal studies, characterized by a 3D network of collagen fibers running in different directions.[2,23–25] A tight adaptation of the CT to the abutment by way of a thin avascular and collagen fiber-rich, scar-like tissue has been already reported. In the present specimens, the CT was composed of collagen fibers running in several directions and, seemingly, functionally organized in a 3D network. Similar results have been reported in other human studies.[5,26] Moreover, under SEM it was possible to observe a dense, chaotic network of fibers running in different but more or less parallel directions to the surface.[27] Similar results were presented by Nevins et al in a human and dog study using implants with a microgrooved collar.[6,8] In these studies, functionally oriented collagen fibers, running toward the grooves of the implant surface, were present, and under SEM, attached collagen fibers were seen. This differentiated network of fibers may have clinical relevance as a mechanical protection of the underlying bone.[5] These human histologic data are extremely valuable to validate and confirm those obtained from studies performed on animal models.

In the present study, the interface between the implants and the surrounding tissues was also directly observable on the same ground sections used by conventional light microscopy. This latter technique has the relative disadvantage of a rather modest resolution, much lower than could be expected by the law of Abbe, a well-known rule of thumb that states that the practical resolution in a section is roughly one tenth of the section thickness, which in this technique is set around 30 µm.[28] The law of Abbe defines the maximum attainable resolution of an optical system as d = 0.5* lambda/NA (where lambda is the wavelength of the light and NA is the numerical aperture of the objective). The SEM has a much higher intrinsic resolution and, at variance with light microscopy, is not affected by the specimen portions that are out-of-focus beneath the surface.

The chemical and physical properties of dental implants created with the DLMF technique have been investigated. The biologic response to the DLMF implant surface has been investigated in different in vitro studies, in which human fibrin clot formation and the behavior of human osteoblasts and mesenchymal stem cells were analyzed.[9–13] The biologic behavior of DLMF implants has been investigated in vivo in different histologic and histomorphometric studies in humans.[9–13] In the present study, the porous surface of the DLMF implants seemed to be conducive to the direct attachment of the collagen fibers on the surface. Indeed, rough surfaces are expected to support a greater adhesion of collagen fibers; however, future clinical randomized studies are underway to better define and evaluate the eventual higher rate of peri-implantitis.

Conclusions

In this study, it was possible to confirm previous data showing that by changing the surface microtexture, it was possible to change the response of the peri-implant soft tissues.

Acknowledgments

This work was partially supported by the Ministry of Education, University and Research (MIUR), Rome, Italy. The authors thank the Large Instruments Centre of Insubria University. The authors reported no conflicts of interest related to this study.

References

1. Glauser R, Schupbach P, Gottlow J, Hammerle CH. Peri-implant soft tissue barrier at experimental one-piece mini-implants with different surface topography in humans: A light microscopic overview and histometric analysis. Clin Implants Dent Relat Res 2005;7(suppl 1): 544–551.
2. Tenenbaum H, Schaaf JF, Cuisinier FJ. Histological analysis of the Ankylos peri-implant tissues in a dog model. Implant Dent 2003;12:259–265.

3. Novaes AB, de Oliveira R, Muglia VA, Papalexiou V, Taba M. The effects of interimplant distances on papilla formation and crestal resorption in implants with a Morse cone connection and a platform switch: A histomorphometric study in dogs. J Periodontol 2006;77:1839–1849.
4. Siar CH, Toh CG, Romanos G, et al. Periimplant soft tissues integration of immediately loaded implants in the posterior macaque mandible: A histomorphometric study. J Periodontol 2003;74:571–578.
5. Schierano G, Ranieri G, Cortese MG, Aimetti M, Preti G. Organization of the connective tissue barrier around long-term loaded implant abutments in man. Clin Oral Implants Res 2002;13:460–464.
6. Nevins M, Nevins ML, Camelo M, Boyesen JL, Kim DM. Human histologic evidence of a connective tissue attachment to a dental implant. Int J Periodontics Restorative Dent 2008;28:111–121.
7. Schupbach P, Glauser R. The defense architecture of the human periimplant mucosa: A histological study. J Prosthet Dent 2007;97(6, suppl):S15–S25.
8. Nevins M, Kim DM, Jun SH, Guze K, Schupbach P, Nevins ML. Histologic evidence of a connective tissue attachment to laser microgrooved abutments: A canine study. Int J Periodontics Restorative Dent 2010;30:245–255.
9. Traini T, Mangano C, Sammons RL, Mangano F, Macchi A, Piattelli A. Direct laser metal sintering as a new approach to fabrication of an isoelastic functionally graded material for manufacture of porous titanium dental implants. Dent Mater 2008;24:525–533.
10. Mangano C, Raspanti M, Traini T, Piattelli A, Sammons R. Stereo imaging and cytocompatibility of a model dental implant surface formed by direct laser fabrication. J Biomed Mater Res Part A 2008;88: 823–831.
11. Mangano C, De Rosa A, Desiderio V, et al. The osteoblastic differentiation of dental pulp stem cells and bone formation on different titanium surface textures. Biomaterials 2010;31:3543–3551.
12. Shibli JA, Mangano C, d'Avila S, et al. Influence of direct laser fabrication implant topography on type IV bone: A histomorphometric study in humans. J Biomed Mater Res Part A 2010;93: 607–614.
13. Mangano C, Piattelli A, d'Avila S, et al. Early human bone response to laser metal sintering surface topography. A histologic report. J Oral Implantol 2010;36:91–96.
14. Piattelli A, Scarano A, Quaranta M. High-precision, cost-effective system for producing thin sections of oral tissues containing dental implants. Biomaterials 1997; 18:577–579.
15. Watzak G, Zechner W, Tangl S, Vasak C, Donath K, Watzek G. Soft tissue around three different implant types after 1.5 years of functional loading without oral hygiene. A preliminary study in baboons. Clin Oral Implants Res 2006;17:229–236.
16. Piattelli A, Scarano A, Piattelli M, Bertolai R, Panzoni E. Histological aspects of the bone and soft tissues surrounding three titanium non-submerged plasma-sprayed implants retrieved at autopsy. A case report. J Periodontol 1997;68:694–700.
17. Gargiulo AW, Wentz FM, Orban B. Dimensions of the dentogingival junction in humans. J Periodontol 1961;32:261–267.
18. Vela-Nebot X, Rodrigue-Ciurana X, Rodado-Alonso C, Segalà-Torres M. Benefits of an implant platform modification technique to reduce crestal bone resorption. Implant Dent 2006;15:313–320.
19. Hermann JS, Buser D, Schenk RK, Cochran DL. Crestal bone changes around titanium implants. A histomorphometric evaluation of unloaded non-submerged and submerged implants in the canine mandible. J Periodontol 2000;71: 1412–1424.
20. Hermann JS, Buser D, Schenk RK, Higginbottom FL, Cochran DL. Biological width around titanium implants. A physiologically formed and stable dimension over time. Clin Oral Impl Res 2000;11:1–11.
21. Cochran DL, Hermann JS, Schenk RK, Higginbottom FL, Buser D. Biological width around titanium implants. A histometric analysis of the implant-gingival junction around unloaded and loaded nonsubmerged implants in the canine mandible. J Periodontol 1997;68: 186–198.
22. Quaranta A, Piattelli A, Scarano A, Quaranta M, Pompa G, Iezzi G. Light-microscopic evaluation of the dimensions of the peri-implant mucosa around immediately loaded and submerged titanium implants in monkeys. J Periodontol 2008; 79:1697–1703.
23. Ericsson I, Berglundh T, Marinello C, Liljenberg B, Lindhe J. Long-standing plaque and gingivitis at implants and teeth in the dog. Clin Oral Implants Res 1992;3:99–103.
24. Arvidson K, Fartash B, Hilliges M, Kondell PA. Histological characteristics of peri-implant mucosa around Branemark and single-crystal sapphire implants. Clin Oral Implants Res 1996;7:1–10.
25. Abrahamsson I, Berglundh T, Wennstrom J, Lindhe J. The peri-implant hard and soft tissues at diffeent implant systems. A comparative study in the dog. Clin Oral Implants Res 1996;7:212–219.
26. Romanos GE, Traini T, Johansson CB, Piattelli A. Biologic width and morphologic characteristics of sioft tissues around immediately loaded implants: Studies performed on human autopsy specimens. J Periodontol 2010;81:70–78.
27. Wennerberg A, Albrektsson T. On implant surfaces: A review of current knowledge and opinions. Int J Oral Maxillofac Implants 2010;25:63–74.
28. Dyer website. http://www.dyergage.com/glossaryTerms.html. Accessed 23 September 2013.